Colloid Transport and Retention in Unsaturated Porous Media: Effect of Colloid Input Concentration

ARTICLE *in* ENVIRONMENTAL SCIENCE AND TECHNOLOGY · JULY 2010

Impact Factor: 5.33 · DOI: 10.1021/es100272f · Source: PubMed

8 AUTHORS, INCLUDING:

Verónica L Morales
ETH Zurich
22 PUBLICATIONS **391** CITATIONS
SEE PROFILE

Larry D. Geohring
Cornell University
45 PUBLICATIONS **546** CITATIONS
SEE PROFILE

J.-Yves Parlange
Cornell University
493 PUBLICATIONS **10,113** CITATIONS
SEE PROFILE

Tammo S Steenhuis
Cornell University
645 PUBLICATIONS **10,324** CITATIONS
SEE PROFILE

Colloid Transport and Retention in Unsaturated Porous Media: Effect of Colloid Input Concentration

WEI ZHANG,[†] VERÓNICA L. MORALES,[†] M. EKREM CAKMAK,[†,§] ANTHONY E. SALVUCCI,[†] LARRY D. GEOHRING,[†] ANTHONY G. HAY,[‡] JEAN-YVES PARLANGE,[†] AND TAMMO S. STEENHUIS*,[†]

Department of Biological and Environmental Engineering, Cornell University, Ithaca, New York 14853, Department of Microbiology, Cornell University, Ithaca, New York 14853, and Department of Environmental Engineering, Cukurova University, Adana, 01330, Turkey

Received January 25, 2010. Revised manuscript received May 11, 2010. Accepted May 26, 2010.

Colloids play an important role in facilitating transport of adsorbed contaminants in soils. Recent studies showed that under saturated conditions colloid retention was a function of its concentration. It is unknown if this is the case under unsaturated conditions. In this study, the effect of colloid concentration on colloid retention was investigated in unsaturated columns by increasing concentrations of colloid influents with varying ionic strength. Colloid retention was observed in situ by bright field microscopy and quantified by measuring colloid breakthrough curves. In our unsaturated experiments, greater input concentrations resulted in increased colloid retention at ionic strength above 0.1 mM, but not in deionized water (i.e., 0 mM ionic strength). Bright field microscope images showed that colloid retention mainly occurred at the solid−water interface and wedge-shaped air−water−solid interfaces, whereas the retention at the grain−grain contacts was minor. Some colloids at the air−water−solid interfaces were rotating and oscillating and thus trapped. Computational hydrodynamic simulation confirmed that the wedge-shaped air−water−solid interface could form a "hydrodynamic trap" by retaining colloids in its low velocity vortices. Direct visualization also revealed that colloids once retained acted as new retention sites for other suspended colloids at ionic strength greater than 0.1 mM and thereby could explain the greater retention with increased input concentrations. Derjaguin−Landau−Verwey−Overbeek (DLVO) energy calculations support this concept. Finally, the results of unsaturated experiments were in agreement with limited saturated experiments under otherwise the same conditions.

Introduction

Understanding colloid transport in unsaturated soils is important because the vadose zone is critical for protecting groundwater (*1*−*3*). To date, the majority of studies have focused on colloid transport in groundwater. Under saturated conditions, colloids are retained at the solid−water interface (SWI) and the wedge-shaped grain−grain contacts (*4*). Recent studies using microscopy in unsaturated media have shown that in addition to the retention sites in saturated soils colloids are retained at the air−water interface (AWI) (*5, 6*) and the air−water−solid (AWS) interfaces (*7*−*9*). Analysis of breakthrough curves (BTCs) from unsaturated columns found that colloid retention depends on properties of porous media and colloids (*10*−*12*), flow regime (*13, 14*), solution chemistry including pH, ionic strength, and organic matter (*15*−*17*), and moisture content (*14, 17, 18*).

Nonetheless, predicting colloid transport in the vadose zone still remains a challenge (*19*). Studies under saturated conditions have shown that increasing input concentrations may either increase or decrease the percentage of retained colloid (*20*−*25*). The decrease in colloid retention is attributed to the occupation of retention sites by colloids, and subsequent "blocking" of additional attachment by electrostatic repulsion of like-charged particles (*25*−*27*). The enhancement in retention is ascribed to "ripening" when interparticle interactions are attractive and the attached colloids become new retention sites for other suspended colloids (*25, 27*−*29*). This concentration effect in saturated media is also related to solution ionic strength (*20*−*22*). Although colloid concentrations in the vadose zone vary by at least 4 orders of magnitude (*2, 4*), the role of colloid input concentration in unsaturated soils has yet to be explored. This gap of knowledge presents a challenge to the prediction of colloid transport in the vadose zone.

To fill the knowledge gap, our objective was to investigate colloid input concentration effect on colloid transport in unsaturated porous media under varying ionic strengths. Additional experiments in saturated media were conducted to confirm the concentration effect observed in unsaturated media. We mainly focused on the experimental and mechanistic aspects of the concentration effect.

Materials and Methods

Sand and Colloid. Red hydrophilic carboxylated polystyrene microspheres with a diameter of 2.6 μm (Magsphere, Inc., Pasdena, CA) were used as model colloids. The colloids supplied in a 10% (w/v) solution (1×10^5 mg L^{-1} or 1×10^{10} colloids mL^{-1}) were washed with deionized (DI) water, and then subsequently diluted to colloid suspensions of 10, 100, and 1000 mg L^{-1} in 0, 0.1, 0.5, and 1.0 mM NaCl solutions. These colloid suspensions were used as influents in the following column experiments. The NaCl solutions free of colloids were used as background influents. Colloid concentration was measured by a spectrophotometer at wavelength of 550 nm (SPECTRONIC 501, Milton Roy, Ivyland, PA) and the calibration curves had a linearity range of 0 to 500 mg L^{-1} ($r^2 = 0.999$).

Angular translucent sand with $d_{10} = 0.27$ mm, $d_{50} = 0.40$ mm, $d_{90} = 0.53$ mm was used (Size 2, AGSCO Corporation, Hasbrouck Heights, NJ), consisting of 99.5% silicon oxide (S_iO_2) and trace amount of aluminum oxide, iron oxide, etc. (Table S1 in Supporting Information S1). The sand was washed with DI water to remove dust, dried, and stored in a closed container. Quartz fragments were liberated from the DI washed sand by sonication in DI water for 30 min, as

* Corresponding author fax: 607 255-4449; tel: 607 255-2489; e-mail: tss1@cornell.edu.
[†] Department of Biological and Environmental Engineering, Cornell University.
[§] Cukurova University.
[‡] Department of Microbiology, Cornell University.

10.1021/es100272f
Published on Web 06/03/2010

TABLE 1. Properties of Background Influents and Electrophoretic Mobility (EM) and ζ-Potential of Quartz Sand and Carboxylated Polystyrene Colloids

IS (mM)	pH	colloids (2.6 μm)		quartz sand	
		EM (μm cm s^{-1} V^{-1})	ζ (mV)	EM (μm cm s^{-1} V^{-1})	ζ (mV)
0	5.9 ± 0.2	−2.86 ± 0.15	−57.2 ± 4.3	−2.42 ± 0.07	−47.5 ± 1.4
0.1	5.9 ± 0.1	−2.54 ± 0.29	−35.4 ± 4.2	−2.69 ± 0.13	−52.8 ± 3.5
0.5	5.9 ± 0.1	−2.24 ± 0.11	−29.7 ± 1.5	−2.79 ± 0.33	−50.3 ± 7.4
1.0	5.8 ± 0.1	−2.11 ± 0.14	−27.9 ± 1.8	−3.01 ± 0.18	−51.7 ± 3.9

TABLE 2. Column Experiment Properties, Effluent Mass Recoveries, and Colloid Deposition Rate Coefficients in Unsaturated and Saturated Media

	IS (mM)	bromide	colloid input concentrations (C_0) (mg L^{-1})		
			10	100	1000
experimental sets	0	expt. thirteen (3)[a]	expt. one (4)	expt. two (3)	expt. three (3)
	0.1		expt. four (5)	expt. five (3)	expt. six (3)
	0.5		expt. seven (4)	expt. eight (2)	expt. nine (2)
	1.0		expt. ten (3)	expt. eleven (2)	expt. twelve (2)
	1.0		expt. fourteen (3)	–	expt. fifteen (2)
moisture content (θ_w)(v/v)	0	0.22 ± 0.04[b]	0.23 ± 0.01	0.22 ± 0.03	0.24 ± 0.04
	0.1	–	0.21 ± 0.04	0.22 ± 0.03	0.23 ± 0.01
	0.5	–	0.21 ± 0.02	0.22 ± 0.02	0.25 ± 0.04
	1.0	–	0.22 ± 0.02	0.24 ± 0.01	0.22 ± 0.03
	1.0	–	0.40 ± 0.00	–	0.40 ± 0.01
pore water velocity (v) (cm min^{-1})	0	0.36 ± 0.07	0.33 ± 0.02	0.34 ± 0.04	0.31 ± 0.05
	0.1	–	0.37 ± 0.08	0.34 ± 0.05	0.32 ± 0.01
	0.5	–	0.36 ± 0.03	0.35 ± 0.04	0.31 ± 0.05
	1.0	–	0.35 ± 0.04	0.31 ± 0.02	0.35 ± 0.05
	1.0	–	0.19 ± 0.00	–	0.19 ± 0.00
effluent recovery (M_{ER})	0	0.95 ± 0.02	0.65 ± 0.09 aA[c]	0.64 ± 0.03 aA	0.68 ± 0.02 aA
	0.1	–	0.41 ± 0.10 aB	0.32 ± 0.04 abB	0.20 ± 0.10 bB
	0.5	–	0.12 ± 0.05 aC	0.07 ± 0.00 abC	0.02 ± 0.01 bC
	1.0	–	0.16 ± 0.02 aC	0.01 ± 0.01 bC	0.00 ± 0.00 bC
	1.0	–	0.14 ± 0.03 aC[d]	–	0.03 ± 0.00 bD[d]
deposition rate coefficient (k_d) (min^{-1})	0	–	0.015 ± 0.005 aA[c]	0.015 ± 0.001 aA	0.012 ± 0.002 aA
	0.1	–	0.036 ± 0.016 aB	0.040 ± 0.010 aB	0.055 ± 0.016 aA
	0.5	–	0.078 ± 0.020 aC	0.093 ± 0.009 abC	0.117 ± 0.013 bB
	1.0	–	0.065 ± 0.006 aC	0.131 ± 0.002 abD	0.204 ± 0.055 bC
	1.0[d]	–	0.038 ± 0.005 aD[d]	–	0.067 ± 0.000 bD[d]

[a] The value in the parentheses is the number of replicates for each experimental set; Expt. 1−13 were conducted in unsaturated media, and Expt. 14−15 were in saturated media. [b] The values are means with one standard deviation. [c] Means of effluent recovery and deposition rate coefficient within a row with different lower case letters are significantly different ($P < 0.05$) under identical IS, and means within a column with different upper case letters are significantly different ($P < 0.05$) under identical C_0. [d] Comparison only made with unsaturated experiments at 1.0 mM (one-tail t-test).

per Saiers and Lenhart (*15*). The quartz suspension was then diluted into the NaCl solutions matching the ionic strength of column influents. By dynamic light scattering, the quartz fragments were sized to be 197 nm in diameter (Zetasizer Nano-ZS, Malvern Instruments Ltd., Malvern, Worcestershire, UK). Electrophoretic mobility (EM) of the colloids and quartz fragments was measured by the zetasizer. The ζ-potential was calculated from the EM values using the tables provided by Ottewill and Shaw (*30*) and is shown in Table 1.

Column Experiments. A transparent, acrylic rectangular column of 10-cm long and 2 × 2-cm wide was wet-packed with the sand to a porosity (θ_0) of 0.40 cm^3 cm^{-3}. Breakthrough experiments of colloid input pulse were conducted under a steady state flow rate (q) of 0.3 mL min^{-1} (i.e., Darcy velocity U= 0.075 cm min^{-1}) and average volumetric moisture content (θ_w) of 0.22 ± 0.03 for unsaturated conditions or 0.40 ± 0.00 for saturated conditions. Fifteen experimental sets were carried out with two to five replications (Table 2). Experimental sets 1−12 were conducted under unsaturated conditions and consisted of three colloid input concentrations (C_0 = 10, 100, 1000 mg L^{-1}) and four ionic strengths (IS = 0, 0.1, 0.5, 1.0 mM). In unsaturated experimental set 13, a pulse of bromide solution (101 mg L^{-1}) was applied instead of the colloids to define the characteristics of water flow in the columns. Experimental sets 14 and 15 were conducted under saturated conditions at C_0 = 10 and 1000 mg L^{-1} and IS = 1.0 mM. Experimental sets were replicated until a definite trend was established. Because colloid retention was more variable at lower C_0 and ionic strength, more replicates were conducted for those experimental sets. Column experiment parameters, including C_0, IS, θ_w, and average pore water velocity ($v = U/\theta_w$), are listed in Table 2.

Hydrodynamic properties of unsaturated columns, including dispersion coefficient (D), mobile water content (θ_m), and Peclet number (Pe), were determined by fitting the bromide breakthrough curves (BTCs) with a physical two-region nonequilibrium model in CXTFIT 2.0 (Supporting Information S2). Colloid transport through porous media at

a steady state can be described by a dispersion−convection equation including a term for first-order colloid deposition (*31*−*33*).

$$\frac{\partial C}{\partial t} = D\frac{\partial^2 C}{\partial z^2} - v\frac{\partial C}{\partial z} - k_d C \quad (1)$$

where C (mg L^{-1}) is the colloid concentration in solution, t (min) is the time, z (cm) is the travel distance, and k_d (min^{-1}) is the colloid deposition rate coefficient. Here, D is obtained from the bromide tests, and v is equal to the average pore water velocity. Because the columns had Peclet number (Pe = 70 ± 25, Table S3) greater than 50, the dispersion term in eq 1 is ignored and the colloid deposition rate coefficient (k_d) (min^{-1}) can thus be determined as follows (*31*−*33*):

$$k_d = -\frac{v}{L}\ln(M_{ER}) \quad (2)$$

where L (cm) is the column length, and M_{ER} is the colloid effluent mass recovery. Here M_{ER} was calculated by numerically integrating the area under the BTCs and then dividing the recovered mass by the input mass.

$$M_{ER} = \frac{\sum_{i=1}[q(t_i - t_{i-1})(C_i + C_{i-1})]}{2t_c q C_0} \quad (3)$$

where t_i is the time lapsed at the ith effluent sample, C_i is the colloid concentration of the ith effluent sample, and t_c is the colloid pulse duration.

Comparisons of k_d and M_{ER} were conducted using the least significant difference (LSD) method in SPSS 17.0 (SPSS Inc., Chicago, IL).

In-situ Visualization of Colloid Transport. Similarly to Morales et al. (*12*), colloid transport was visualized in situ by digital bright field microscopy (BFM) (KH-7700, Hirox-USA, River Edge, NJ). The BFM lens was mounted horizontally to visualize the pore-scale processes from a lateral view of the columns. Images and videos were periodically taken at pores located 2−3 cm from the column top.

DLVO Energy Calculations and Hydrodynamic Simulation. Colloid retention greatly depends on total Derjaguin−Landau−Verwey−Overbeek (DLVO) interaction energy of colloid interacting with other colloids or interfaces (e.g., SWI or AWS interfaces) in soil pores (*4*). In the DLVO energy profile, the negative interaction energy at primary energy minimum or secondary energy minimum indicates an attractive force that may result in colloid aggregation or attachment, while the positive energy means a repulsive force that promotes the colloid stability or mobility. Thus, total DLVO interaction energies were calculated as the sum of Lifshitz−van der Waals, electric double layer, and Born repulsion interactions for colloid−SWI, colloid−colloid, and colloid−AWI interactions. Born repulsion was included to account for the interaction energy resulting from the overlap of the electron clouds of atoms, similar to the approach of Hahn et al. (*34*). Attachment efficiency (α) determining whether particle collision with the interfaces results in attachment was estimated from DLVO energies using a Maxwell model (Supporting Information S3).

Colloid retention is also highly dependent on pore-scale hydrodynamics (*35*−*37*). To explain the observed colloid retention at the AWS interfaces, two-dimensional flow field in the wedge-shaped AWS interface formed by a sand grain and a meniscus was simulated by numerically solving the Stokes and continuity equations using COMSOL Multiphysics v3.5a software package (COMSOL, Inc., Burlington, MA). A nonslip boundary (i.e., zero velocity) was set at the sand surface, whereas a slip boundary (i.e., the normal component of velocity is zero and the tangential component of total stress is zero) was defined at the meniscus. More detailed information about the experimental conditions, the DLVO calculations, and the hydrodynamic simulation are provided in the Supporting Information.

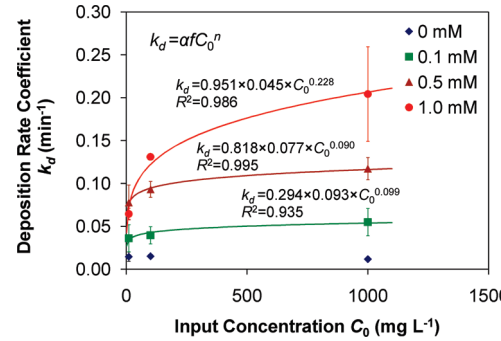

FIGURE 1. Colloid deposition rate coefficients as a function of colloid input concentration and ionic strength in unsaturated media. In the equation, α is attachment efficiency, and *f* and *n* are fitting parameters (Supporting Information S3).

Results

Column Breakthrough Experiment. The bromide BTCs in unsaturated columns were best fitted with a physical two-region nonequilibrium model ($R^2 > 0.992$). The results showed that 63 ± 9% of water in the unsaturated columns were mobile and 37 ± 9% of water located in small pores or wedges were immobile or stagnant (Table S3), which agrees with the value in the literature (*14*). The conservative bromide was eluted almost completely with an effluent mass recovery of 95 ± 2% (Table 2).

Colloid mass recoveries in effluent (M_{ER}) and deposition rate coefficients (k_d) for the unsaturated and saturated columns based on the BTCs (Figure S1) are presented in Table 2 and Figure 1. As expected (*1, 3, 4, 15, 29*), these results confirmed that increasing ionic strength significantly enhanced colloid retention (Table 2, Figure 1). Additionally, when input concentrations increased, the effluent mass recovery decreased and colloid retention increased at ionic strength of 0.1 mM or greater. At any nonzero ionic strength k_d is a power function of input concentrations (Figure 1). The greater the influent ionic strength, the stronger effect the concentration had on colloid retention, judging from the greatest exponent of the regression at 1 mM ionic strength. In saturated experiments, colloid retention was less than that of unsaturated experiments (*17, 18*), and similarly increased with input concentrations (Table 2).

DLVO Energy Profiles. A negative primary or secondary energy minimum in the DLVO energy profiles is required for colloids to be attracted to grain surfaces or other colloids. The DLVO energy profiles in Figure 2 for colloid−SWI and colloid−colloid interactions indicate that a negative primary energy minimum does not exist. Secondary energy minima exist for ionic strength of 0.1 mM or greater, but not for the 0 mM solutions. Because the depth of the secondary minimum increases with ionic strength (Figure 2), colloids become more attracted to other colloids or grains as ionic strength increases. The attachment efficiency (α) for colloid−SWI interactions increased from 0 at 0 mM to 0.294 at 0.1 mM, 0.818 at 0.5 mM, and 0.951 at 1 mM. The similar trend was observed for colloid−colloid interactions (Table S4). Colloids are not attracted to the AWI at any ionic strength (Figure S3), resulting in zero attachment efficiency.

Colloid Retention: Visualization. Images of colloid retained in unsaturated columns after the colloid pulse confirmed that more colloids can be retained at greater ionic strength (Figure 3). Although the retention at the grain−grain

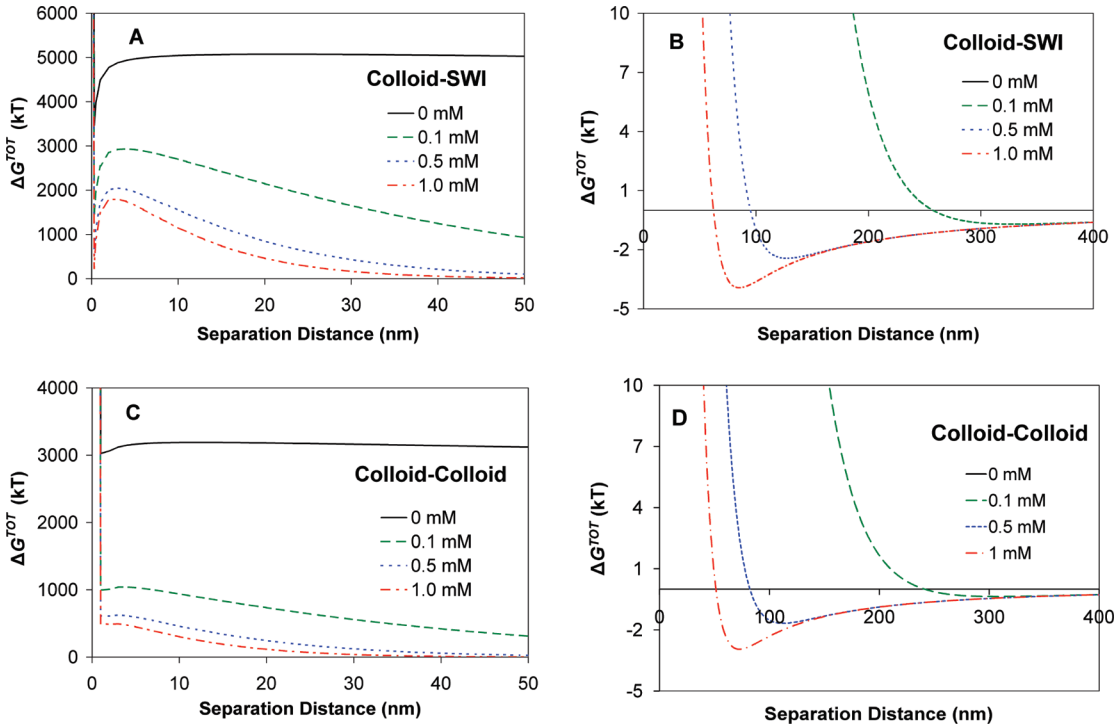

FIGURE 2. Total DLVO interaction energy (ΔG^{TOT}) for a colloid interacting with the solid−water interface (SWI) and another colloid: (A) primary energy barrier for colloid−SWI interaction; (B) second energy minimum for colloid−SWI interaction; (C) primary energy barrier for colloid−colloid interaction; (D) secondary energy minimum for colloid−colloid interaction.

contacts existed, it appeared minor compared with the retention at the SWI and AWS interfaces (Figure 3). The retention at the SWI and AWS interface becomes more dominant as the ionic strength increases (Figure 3). In saturated conditions, colloid retention occurred both at the SWI and the grain−grain contacts, with the SWI being the dominant retention site (Figure 3E). More visuals are provided in Supporting Information S5 including 3 video clips (Table S5). To aid in interpretation, Figure 4 schematically shows the four observed retention sites.

In the wedge-shaped AWS pore space loosely retained colloids were observed to spin or oscillate (*V1.mpg* in Supporting Information S5). At the SWI colloids were retained in strips or patches, whereas at wedge-shaped grain−grain contacts and AWS interfaces the retained colloids formed aggregates as shown in Figure 3, Figure S5A, and *V2.mpg*. Additionally, mobile colloids were filtered by amorphous colloid aggregates in the AWS interfaces, and suspended colloids attached to the previously immobilized colloids and formed a thick colloid strip on the SWI as shown in *V2.mpg* and *V3.mpg*.

Discussion

Colloid Retention Sites: Mechanisms. In this section, we will first discuss the retention sites involving only the grain surfaces and water phase, thus common to both saturated and unsaturated media. Then, we will discuss the sites relating to the air phase. Elucidation of these retention mechanisms is advantageous in explaining the observed concentration effect.

Colloid retention at the grain surface (i.e., the SWI) is common in both saturated and unsaturated media. Relatively more colloids are retained at the SWI as ionic strength increases (Figure 3), because the interface becomes more attractive to colloids, shown by the increasing depth of secondary energy minimum (Figure 2). Colloid retention at the SWI by the secondary energy minimum has been well established (*16, 34, 38*). Despite having a repulsive colloid−SWI interaction at IS = 0 mM (no secondary energy minimum in Figure 2B), a small amount of colloid was retained (Figure 3A). It is known that natural sand surfaces are typically coated with patchy Al or Fe oxides that carry positive charges at neutral pH (*29, 39, 40*) and could act as retention sites for colloids. To test this hypothesis, a subsample of the sand was cleaned by HNO_3 acid wash to remove Al and Fe oxides. The ζ-potential of that sand surface was much more negative than the only water washed sand (Table 1 and Table S2), implying that Al or Fe oxides indeed provide positive charge sites. At greater ionic strength, the retention by patchy oxides is masked by retention at the secondary energy minimum.

Colloid retention also occurred at the grain−grain contacts in both saturated and unsaturated media (Figure 3, and *V2.mpg*). In saturated media, the colloid retention at the wedge-shaped grain−grain contacts under unfavorable attachment conditions (i.e., in the presence of an energy barrier) has been reported and attributed to straining or wedging (*4, 35, 41*). The flow funneling and low velocity vortices (i.e., the flow stagnation zone) in the grain−grain contacts facilitate colloid straining or wedging in this pore space (*35−37*). The number of colloids transported to these regions depends on the attraction energy between the grain surface and colloids (e.g., the secondary energy minimum) (*37*). When colloids become easily attracted to the grain surface, the grain−grain contacts become a less important retention site (*35*), which agrees with our observation.

Colloid retention in the AWS interfaces occurs uniquely in unsaturated media. The retention at the AWS interfaces in this study cannot be explained by capillary force previously suggested (*42−44*), because the colloids cannot penetrate the air−water interface due to the high DLVO energy barrier for colloid−AWI interaction and the stable menisci at the steady state conditions (Figure S3). We observed that some colloids were trapped in the vortices of low velocity in the wedges of the AWS interfaces because loosely retained colloids were spinning or oscillating as shown in *V1.mpg*. To explain this observation, we simulated the flow field in this region with a nonslip boundary at the grain surface and a slip boundary at the meniscus using COMSOL. The wedge-

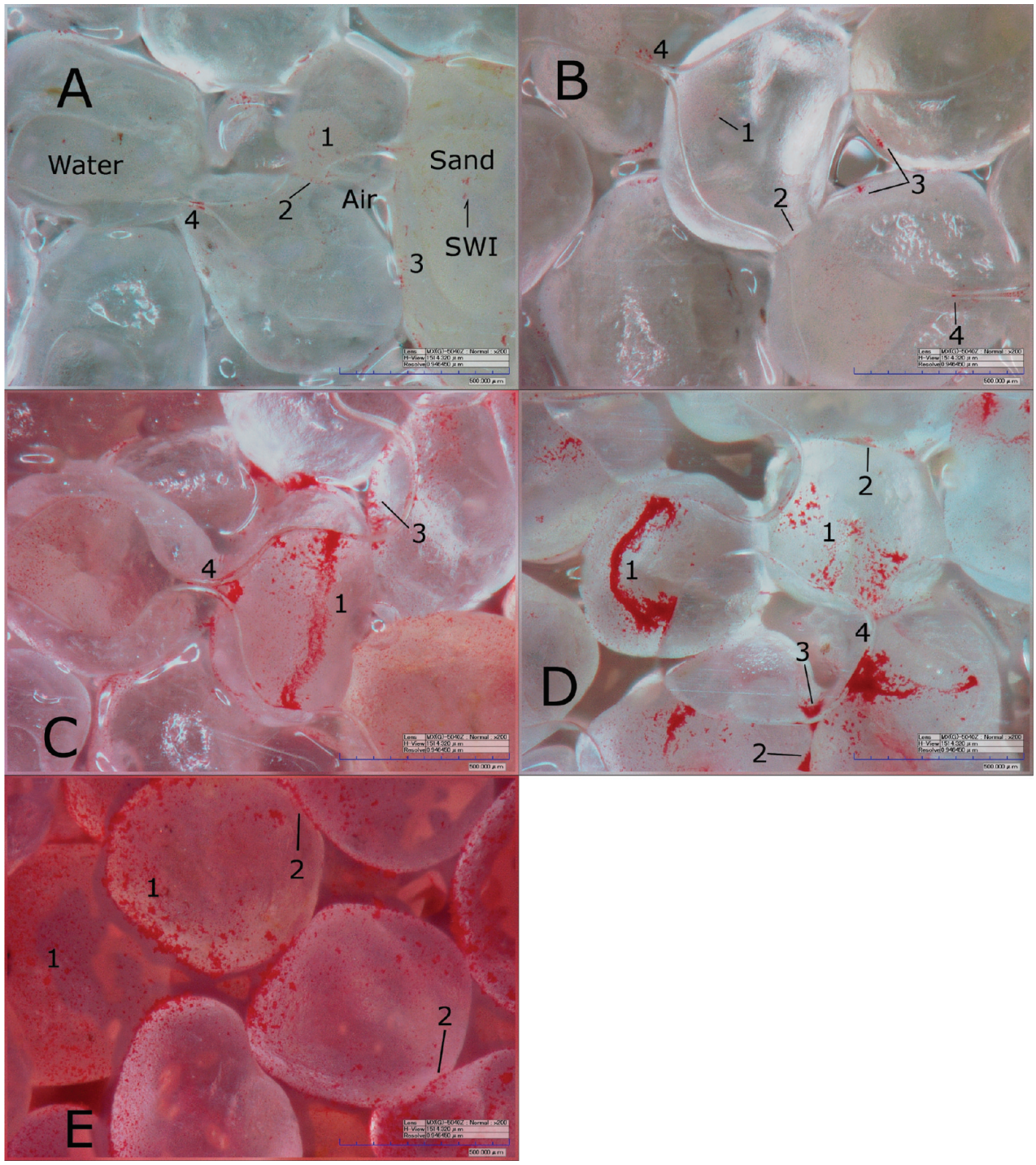

FIGURE 3. Observed retention sites of colloids in unsaturated (A, B, C, D) and saturated (E) experiments with C_0 = 1000 mg L^{-1} under four ionic strengths (IS): (A) IS = 0 mM; (B) IS = 0.1 mM; (C) IS = 0.5 mM; (D) IS = 1.0 mM; (E) IS = 1.0 mM. Retention site 1 = the solid−water interface (SWI), 2 = the grain−grain contacts, 3 = the air−water−solid (AWS) interface, 4 = the AWS pore space formed by the adjacent menisci and the SWI, a particular case of site 3. Microscopic view is rotated 90 counterclockwise due to horizontal mounting of the microscope lens. The flow direction was from left and right, representing the downward flow in the column experiments. Scale bar = 500 μm.

shaped pore space caused immobile regions near the gaps between the grain and the meniscus, where water, instead of mixing with the bulk flow, rotates in an infinite set of nested ring vortices of low velocity (Figure 5). Also, the flow is funneled into the wedge-shaped pore space clearly shown by the streamlines in Figure 5. This is similar to the flow pattern in the wedge at the grain−grain contacts in saturated media (*36*), validated by the COMSOL simulation with two nonslip boundaries at the grain surfaces (*37*). The existence of this flow stagnation zone also resonates with the 37 ± 9% immobile water fraction estimated from the bromide tests (Table S3). Thus, the flow funneling and the vortices of low velocity at the wedge-shaped AWS interfaces were partially responsible to the observed retention. Additionally, the hydrodynamic factors are coupled with the DLVO secondary energy minimum, which together determines the number of colloids transported to and the formation of colloid aggregates at this region (*4, 36, 37, 45, 46*).

Concentration Dependence of Colloid Retention. In addition to the enhanced retention with greater ionic

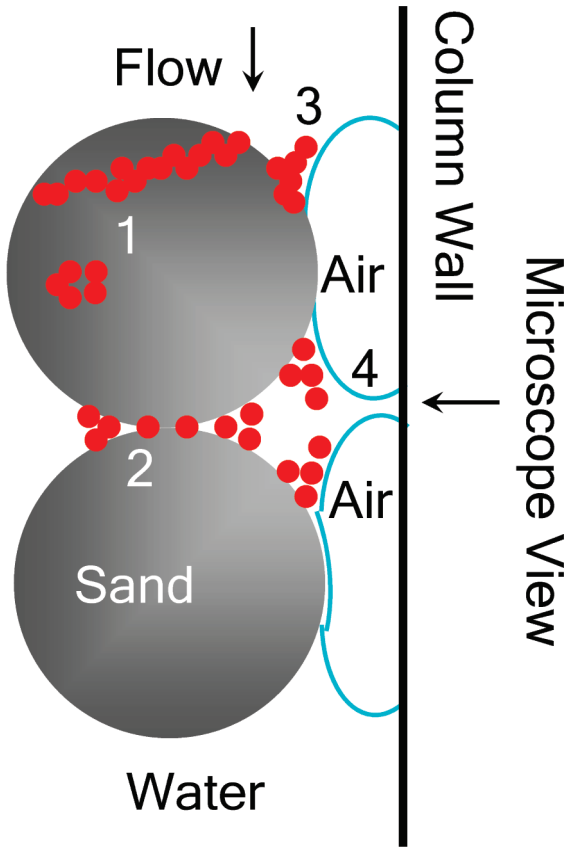

FIGURE 4. Schematic of colloid retention sites in unsaturated media: (1) the SWI; (2) the grain−grain contacts; (3) the AWS interface; (4) the AWS pore space formed by the adjacent menisci and the SWI.

strength, colloid retention increases with input concentrations at nonzero ionic strength (Figure 1). This concentration effect has to be related to the SWI and the AWS interfaces because they are the dominant retention sites. As shown in the video suspended colloids are "captured" by already retained colloids at the SWI and AWS interfaces. The DLVO colloid−colloid interactions indicate that colloids may attach to each other at the secondary energy minima at nonzero ionic strength (Figure 2). The initial colloid retention might be proportional to colloid concentrations in solution, and the consequent capture should become more effective as the retention sites grow (Figure 1), resulting in increased overall attachment efficiency (*25*). At greater input concentration the growth of retention sites is faster, thus could partially explain the observed concentration effect. Additionally, colloid aggregation in the bulk solution could be a factor as well. At the zero ionic strength, this ripening-type effect was absent due to the repulsive intraparticle interaction (Figure 2).

This coupling of the concentration effect with ionic strength has only been reported in saturated media (*20*−*22*). Gannon et al. (*20*) and Tan et al. (*21*) observed that bacteria (*Pseudomonas sp.* strain KL2) retention decreased as its input concentration increased from 10^8 cells mL^{-1} to 10^9 cell mL^{-1} in 10 mM NaCl solution, but remained unchanged in DI water. This was attributed to the filling of the finite retention sites controlled by ionic strength. Bradford et al. (*22*) reported that the concentration effect of carboxylated polystyrene colloids was absent at both low and high ionic strength (6 and 106 mM), but became evident at the intermediate ionic strength (31 and 56 mM). Here we showed the concentration effect of carboxylated polystyrene colloids at ionic strength of 0.1 mM or greater due to reduced electrostatic repulsion from the relative small ζ-potential (Table 1).

In saturated media increasing input concentration was reported to cause lower retention of several bacteria strains and carboxylated polystyrene colloids (*20*−*24*). The opposite was observed for bacteria *Pseudomonas florescens* P17 (*25*), which agrees with our results. Since Bradford et al. (*22*) used colloids similar to those of this study we were able to cross-compare with their results. Compared with this study using angular quartz sand at near-neutral pH of 6−7, Bradford et al. (*22*) observed the opposite concentration effect in saturated spheroidal quartz sand at pH 10. The water saturation degree cannot explain the discrepancy, because our saturated experiments gave similar results with the

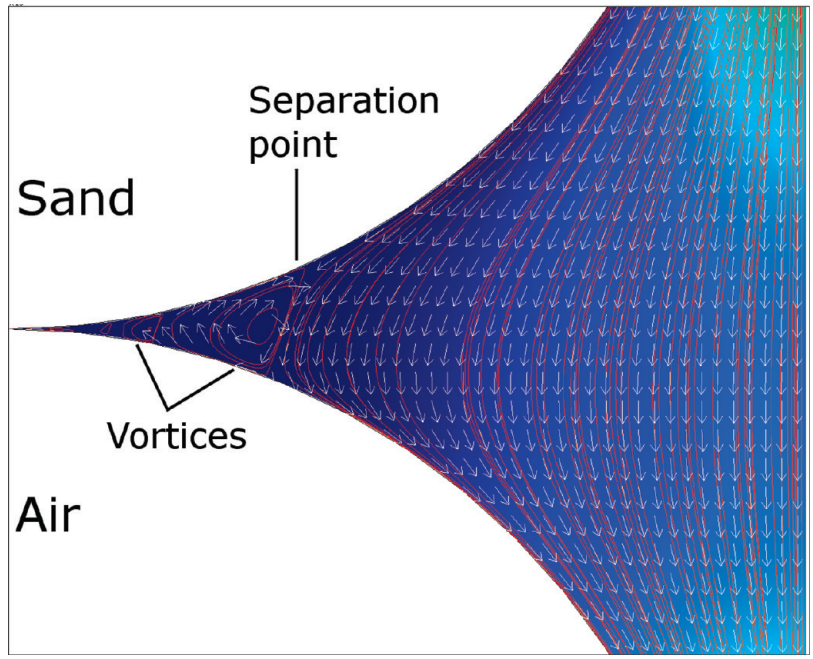

FIGURE 5. Simulated flow velocity field at the wedge-shaped air−water−solid (AWS) interface. Separation of streamlines (red lines) from the sand and meniscus surface creates an immobile region with vortices where water rotates as shown by the normalized water velocity (white arrows).

unsaturated experiments. Rather the discrepancy stems from the difference in the system pH, surface potential of colloids and sands, and grain shape. The ζ-potential of their colloid and sand were more negative and the Fe and Al oxides were negatively charged at pH 10, which resulted in greater electrostatic repulsion. The angularity of our sand could also contribute to the greater colloid aggregation and ripening (*46*).

Finally, Tong et al. (*46*) conjectured that in saturated media the flow funneled to the grain−grain contacts may induce colloid aggregation (or ripening). Similarly, the funneling flow toward the AWS interfaces shown in Figure 5 could play an equal role in unsaturated media. In light of the above discussion, the concentration dependence of colloid retention in unsaturated porous media depends on intricate interplays of solution chemistry (e.g., ionic strength and pH), hydrodynamics, and properties of porous media and colloids (e.g., surface potential and grain shape).

Implications. The findings of this study have interesting implications to the transport of microorganisms, abiotic colloids, and colloid-associated contaminants in the vadose zone. Because more colloids are retained at greater ionic strength, the greatest transport will occur with rainfall that has a lower ionic strength than soil solution. Additionally, the concentration effect, intriguingly, implies that colloids are less well retained in the subsoil where the concentration is lower, because most surface-originated colloids are being retained at the topsoil. This dependence is often not included in models, which may underpredict the risk of groundwater contamination. For a pathogen with a low infectious dose (e.g., *Cryptosporidium parvum*) improving the prediction of colloid transport is desirable.

Acknowledgments

This research was funded by National Science Foundation (0635954), Binational Agricultural Research and Development Fund (IS-3962-07), and U.S. Department of Agriculture.

Supporting Information Available

S1 Properties of the quartz sand; S2 column experiments; S3 DLVO energy calculations and deposition rate coefficient; S4 hydrodynamic simulation; S5 in-situ visualization of colloid transport (3 figures and 3 video clips). This material is available free of charge via the Internet at http://pubs.acs.org.

Literature Cited

(1) de Jonge, L. W.; Kjaergaard, C.; Moldrup, P. Colloids and colloid-facilitated transport of contaminants in soils: an introduction. *Vadose Zone J.* **2004**, *3*, 321–325.

(2) DeNovio, N. M.; Saiers, J. E.; Ryan, J. N. Colloid movement in unsaturated porous media: recent advances and future directions. *Vadose Zone J.* **2004**, *3*, 338–351.

(3) McCarthy, J. F.; McKay, L. D. Colloid transport in the subsurface: past, present, and future challenges. *Vadose Zone J.* **2004**, *3*, 326–337.

(4) Bradford, S. A.; Torkzaban, S. Colloid transport and retention in unsaturated porous media: a review of interface-, collector-, and pore-scale processes and models. *Vadose Zone J.* **2008**, *7* (2), 667–681.

(5) Wan, J.; Wilson, J. L. Visualization of the role of the gas-water interface on the fate and transport of colloids in porous media. *Water Resour. Res.* **1994**, *30* (1), 11–23.

(6) Wan, J.; Wilson, J. L. Colloid transport in unsaturated porous media. *Water Resour. Res.* **1994**, *30* (4), 857–864.

(7) Crist, J. T.; McCarthy, J. F.; Zevi, Y.; Baveye, P.; Throop, J. A.; Steenhuis, T. S. Pore-scale visualization of colloid transport and retention in partly saturated porous media. *Vadose Zone J.* **2004**, *3*, 444–450.

(8) Crist, J. T.; Zevi, Y.; McCarthy, J. F.; Throop, J. A.; Steenhuis, T. S. Transport and retention mechanisms of colloids in partially saturated porous media. *Vadose Zone J.* **2005**, *4*, 184–195.

(9) Zevi, Y.; Dathe, A.; McCarthy, J. F.; Richards, B. K.; Steenhuis, T. S. Distribution of colloid particles onto interfaces in partially saturated sand. *Environ. Sci. Technol.* **2005**, *39* (18), 7055–7064.

(10) Zhuang, J.; Qi, J.; Jin, Y. Retention and transport of amphiphilic colloids under unsaturated flow conditions: Effect of particle size and surface property. *Environ. Sci. Technol.* **2005**, *39* (20), 7853–7859.

(11) Gargiulo, G.; Bradford, S.; Šimůnek, J.; Ustohal, P.; Vereecken, H.; Klumpp, E. Bacteria transport and deposition under unsaturated conditions: the role of the matrix grain size and the bacteria surface protein. *J. Contam. Hydrol.* **2007**, *92*, 255–273.

(12) Morales, V. L.; Gao, B.; Steenhuis, T. S. Grain surface-roughness effects on colloid retention in the vadose zone. *Vadose Zone J.* **2009**, *8* (1), 11–20.

(13) Saiers, J. E.; Lenhart, J. J. Colloid mobilization and transport within unsaturated porous media under transient-flow conditions. *Water Resour. Res.* **2003**, *39* (1), 1019,; doi:10.1029/2002WR001370.

(14) Gao, B.; Saiers, J. E. Pore-scale mechanisms of colloid deposition and mobilization during steady and transient flow through unsaturated granular media. *Water Resour. Res.* **2006**, *42*, W01410,; doi:10.1029/2005WR004233.

(15) Saiers, J. E.; Lenhart, J. J. Ionic strength effects on colloid transport and interfacial reactions in partially saturated porous media. *Water Resour. Res.* **2003**, *39* (9), 1256,; doi:10.1029/2002WR001887.

(16) Franchi, A.; O'Melia, C. R. Effects of natural organic matter and solution chemistry on the deposition and reentrainment of colloids in porous media. *Environ. Sci. Technol.* **2003**, *37* (6), 1122–1129.

(17) Torkzaban, S.; Bradford, S. A.; van Genuchten, M. T.; Walker, S. L. Colloid transport in unsaturated porous media: the role of water content and ionic strength on particle straining. *J. Contam. Hydrol.* **2008**, *96*, 113–127.

(18) Powelson, D. K.; Mills, A. L. Transport of *Escherichia coli* in sand columns with constant and changing water contents. *J. Environ. Qual.* **2001**, *30*, 238–245.

(19) Flury, M.; Qiu, H. Modeling colloid-facilitated contaminant transport in the vadose zone. *Vadose Zone J.* **2008**, *7* (2), 682–697.

(20) Gannon, J.; Tan, Y.; Baveye, P.; Alexander, M. Effect of sodium chloride on transport of bacteria in a saturated aquifer material. *Appl. Environ. Microbiol.* **1991**, *57* (9), 2497–2501.

(21) Tan, Y.; Gannon, J. T.; Baveye, P.; Alexander, M. Transport of bacteria in an aquifer sand: experiments and model simulations. *Water Resour. Res.* **1994**, *30* (12), 3243–3252.

(22) Bradford, S. A.; Kim, H. N.; Haznedaroglu, B. Z.; Torkzaban, S.; Walker, S. L. Coupled factors influencing concentration-dependent colloid transport and retention in saturated porous media. *Environ. Sci. Technol.* **2009**, *43* (18), 6996–7002.

(23) Bradford, S. A.; Bettahar, M. Concentration dependent transport of colloids in saturated porous media. *J. Contam. Hydrol.* **2006**, *82*, 99–117.

(24) Haznedaroglu, B. Z.; Kim, H. N.; Bradford, S. A.; Walker, S. L. Relative transport behavior of *Escherichia coli* O157:H7 and *Salmonella enterica* Serovar Pullorum in packed bed column systems: influences of solution chemistry and cell concentration. *Environ. Sci. Technol.* **2009**, *43* (6), 1838–1844.

(25) Camesano, T. A.; Logan, B. E. Influence of fluid velocity and cell concentration on the transport of motile and nonmotile bacteria in porous media. *Environ. Sci. Technol.* **1998**, *32* (11), 1699–1708.

(26) Ko, C.-H.; Elimelech, M. The "shadow effect" in colloid transport and deposition dynamics in granular porous media: measurement and mechanisms. *Environ. Sci. Technol.* **2000**, *34* (17), 3681–3689.

(27) Song, L.; Elimelech, M. Dynamics of colloid deposition in porous media: modeling the role of retained particles. *Colloid Surf., A* **1993**, *73*, 49–63.

(28) Darby, J. L.; Lawler, D. F. Ripening in depth filtration: Effect of particle size on removal and head loss. *Environ. Sci. Technol.* **1990**, *24* (7), 1069–1079.

(29) Liu, D.; Johnson, P. R.; Elimelech, M. Colloid deposition dynamics in flow through porous media: Role of electrolyte concentration. *Environ. Sci. Technol.* **1995**, *29* (12), 2963–2973.

(30) Ottewill, R. H.; Shaw, J. N. Electrophoretic studies on polystyrene latices. *J. Electroanal. Chem. Interfacial Electrochem.* **1972**, *37*, 133–142.

(31) Kretzschmar, R.; Sticher, H. Transport of humic-coated iron oxide colloids in a sandy soil: Influence of Ca^{2+} and trace metals. *Environ. Sci. Technol.* **1997**, *31* (12), 3497–3504.

(32) Kretzschmar, R.; Barmettler, K.; Grolimund, D.; Yan, Y.-D.; Borkovec, M.; Sticher, H. Experimental determination of colloid deposition rates and collision efficiencies in natural porous media. *Water Resour. Res.* **1997**, *33* (5), 1129–1137.

(33) Akbour, R. A.; Douch, J.; Hamdani, M.; Schmitz, P. Transport of kaolinite colloids through quartz sand: Influence of humic acid, Ca^{2+}, and trace metals. *J. Colloid Interface Sci.* **2002**, *253*, 1–8.

(34) Hahn, M. W.; Abadzic, D.; O'Melia, C. R. Aquasols: On the role of secondary minima. *Environ. Sci. Technol.* **2004**, *38* (22), 5915–5924.

(35) Johnson, W. P.; Tong, M.; Li, X. On colloid retention in saturated porous media in the presence of energy barriers: the failure of α, and opportunities to predict *η*. *Water Resour. Res.* **2007**, *43*, W12S13,; doi:10.1029/2006WR005770.

(36) Bradford, S. A.; Torkzaban, S.; Leij, F.; Šimůnek, J.; van Genuchten, M. T. Modeling the coupled effects of pore space geometry and velocity on colloid transport and retention. *Water Resour. Res.* **2009**, *45*, W02414,; doi:10.1029/2008WR007096.

(37) Torkzaban, S.; Tazehkand, S. S.; Walker, S. L.; Bradford, S. A. Transport and fate of bacteria in porous media: coupled effects of chemical conditions and pore space geometry. *Water Resour. Res.* **2008**, *44*, W04403,; doi:10.1029/2007WR006541.

(38) Hahn, M. W.; O'Melia, C. R. Deposition and reentrainment of Brownian particles in porous media under unfavorable chemical conditions: Some concepts and applications. *Environ. Sci. Technol.* **2004**, *38* (1), 210–220.

(39) Johnson, R. R.; Sun, N.; Elimelech, M. Colloid transport in geochemically heterogeneous porous media: Modeling and measurements. *Environ. Sci. Technol.* **1996**, *30* (11), 3284–3293.

(40) Ryan, J. N.; Elimelech, M. Colloid mobilization and transport in groundwater. *Colloids Surf., A* **1996**, *107*, 1–56.

(41) Bradford, S. A.; Šimůnek, J.; Bettahar, M.; van Genuchten, M. T.; Yates, S. R. Significance of straining in colloid deposition: evidence and implications. *Water Resour. Res.* **2006**, *42*, W12S15,; doi:10.1029/2005WR004791.

(42) Steenhuis, T. S.; Dathe, A.; Zevi, Y.; Smith, J. L.; Gao, B.; Shaw, S. B.; DeAlwis, D.; Amaro-Garcia, S.; Fehrman, R.; Cakmak, M. E.; et al. Biocolloid retention in partially saturated soils. *Biologia* **2006**, *61*, S229–S233.

(43) Gao, B.; Steenhuis, T. S.; Zevi, Y.; Morales, V. L.; Nieber, J. L.; Richards, B. K.; McCarthy, J. F.; Parlange, J.-Y. Capillary retention of colloids in unsaturated porous media. *Water Resour. Res.* **2008**, *44*, W04504,; doi:10.1029/2006WR005332.

(44) Shang, J.; Flury, M.; Deng, Y. Force measurements between particles and the air-water interface: implications for particle mobilization in unsaturated porous media. *Water Resour. Res.* **2009**, *45*, W06420,; doi:10.1029/2008WR007384.

(45) Bradford, S. A.; Torkzaban, S.; Walker, S. L. Coupling of physical and chemical mechanisms of colloid straining in saturated porous media. *Water Res.* **2007**, *41*, 3012–3024.

(46) Tong, M.; Ma, H.; Johnson, W. P. Funneling of flow into grain-to-grain contacts drives colloid-colloid aggregation in the presence of an energy barrier. *Environ. Sci. Technol.* **2008**, *42* (8), 2826–2832.

ES100272F